Terahertz spectroscopy of electromagnons in Eu1−xYxMnO3

Andrei Pimenov, Alois Loidl, A. A. Mukhin, V. D. Travkin, V. Yu. Ivanov, A. M. Balbashov

Angaben zur Veröffentlichung / Publication details:

Pimenov, Andrei, Alois Loidl, A. A. Mukhin, V. D. Travkin, V. Yu. Ivanov, and A. M. Balbashov. 2008. "Terahertz spectroscopy of electromagnons in Eu1−xYxMnO3." *Physical Review B* 77 (1): 014438. https://doi.org/10.1103/physrevb.77.014438.

Terahertz spectroscopy of electromagnons in $Eu_{1-x}Y_xMnO_3$

A. Pimenov,[1] A. Loidl,[2] A. A. Mukhin,[3] V. D. Travkin,[3] V. Yu. Ivanov,[3] and A. M. Balbashov[4]
[1]*Experimentelle Physik IV, Universität Würzburg, 97074 Würzburg, Germany*
[2]*Experimentalphysik V, EKM, University of Augsburg, 86135 Augsburg, Germany*
[3]*General Physics Institute of the Russian Academy of Sciences, 119991 Moscow, Russia*
[4]*Moscow Power Engineering Institute, 105835 Moscow, Russia*
(Received 24 July 2007; published 30 January 2008)

Dielectric permittivity spectra of yttrium-doped $EuMnO_3$ in the composition range $0 \leqslant x \leqslant 0.5$ have been investigated in the terahertz frequency range. Magnetoelectric contributions to the permittivity were observed in all compositions for ac electric fields parallel to the crystallographic *a* axis. Well-defined electromagnons exist for $x \geqslant 0.2$ close to $\nu \sim 20$ cm^{-1} and with dielectric strength strongly increasing on doping. In addition to electromagnons, a broad contribution of magnetoelectric origin is observed for all compositions. For $Eu_{0.8}Y_{0.2}MnO_3$, the electromagnons can be suppressed by external magnetic fields which induce a canted antiferromagnetic phase. Magnetoelectric effects in the different doping regimes are discussed in detail.

DOI: 10.1103/PhysRevB.77.014438 PACS number(s): 75.47.Lx, 75.80.+q, 75.30.Ds

I. INTRODUCTION

Electric and magnetic properties in most cases are well separated in the physics of the solid state. However, as can be expected from the Maxwell equations, the cross-coupling effects between electricity and magnetism may exist under appropriate symmetry conditions. This cross coupling has been pointed out already by Curie[1] and was later called magnetoelectric (ME) effect. ME effect can be observed as changes in the electric polarization in external magnetic fields or as electric-field dependence of the magnetic moment.

In spite of early prediction of the ME effect, experimentally, this effect could not be confirmed during more than half a century. The breakthrough came after Landau and Lifshitz[2] showed that ME contribution is only possible in time-asymmetric media, which is realized, e.g., in magnetically ordered samples. This lead to the prediction[3] of the time asymmetry in Cr_2O_3 and to the experimental observation[4] of a field-induced polarization in this compound. The review of the earlier works on this topic can be found in Refs. 5 and 6.

Recent revival of the interest to the ME effect[7–10] can be connected with an additional microscopic mechanism of the magnetoelectricity: incommensurate magnetic structure can favor for ME interaction under suitable symmetry. Due to the relative "weakness" of the incommensurate magnetic configuration against external magnetic fields, dielectric and ferroelectric properties in such systems can be controlled by moderate magnetic fields. Such spin-driven ferroelectricity has been shown to be operative in $Ni_3V_2O_8$.[11] In some perovskite manganites such as $TbMnO_3$ or $GdMnO_3$, it was proven experimentally[12,13] that the onset of helical magnetic order induces spontaneous ferroelectric (FE) polarization.[14,15] Dzyaloshinskii-Moriya-type interactions have been utilized to explain the ferroelectricity which is induced by the helical spin structure.[16–18]

Among the systems revealing the ME effect, special interest is drawn to materials with the simultaneous occurrence of (anti)ferromagnetism and ferroelectricity, which are termed multiferroics.[19] In addition to unusual physical properties, the multiferroics are also attractive from the point of view of possible applications,[7] e.g., as memory elements and optical switches. Multiferroic behavior occurs in a variety of systems originating from very different physical mechanisms, including materials with independent magnetic and ferroelectric subsystems, such as some boracites, Aurivillius phases, hexagonal manganites, and the lone-pair ferroelectrics with magnetic ions.[8]

The existence of an additional energy scale in ME compounds can lead to the appearance of a corresponding excitation of ME origin.[5,20,21] Recently, such excitations, called electromagnons, have been observed experimentally[22,23] and it has been shown that electromagnons are the relevant collective ME modes in these materials. Electromagnons are strongly renormalized spin waves which are coupled to optical phonons and can be excited by an ac electric field. In $TbMnO_3$ and $GdMnO_3$, it has been documented that these new excitations exist not only in the magnetic phase characterized by the helical spin structure but also in the longitudinally modulated (sinusoidal) structure, provided that a "helical-type" vector component of the spin wave is dynamically induced via the ac electric field.[22,24] The appearance of electromagnons is supported by a theoretical modeling of elementary excitations in helical magnets[21] and by a polaron-like excitation scheme of coupled phonons and magnons.[25] In addition to renormalized phonons, an excitation has been predicted for the ME state which originates from magnons and reveals a frequency proportional to $\sqrt{SJD}$, where S is the spin value, J the exchange coupling, and D the magnetic anisotropy. The coupling between electromagnons and phonons has been verified experimentally for $GdMnO_3$ (Ref. 24) and for $Eu_{0.75}Y_{0.25}MnO_3$.[26]

The analysis of the excitations in perovskite multiferroics such as $TbMnO_3$ still remains complicated due to the interplay between the magnetic sublattices of the manganese and of the rare earth ions. Further difficulties arise, e.g., in $GdMnO_3$, as this compound is close to a metastable ground state[24,27] and can hardly be investigated using neutron scattering due to strong absorption. Therefore, the details of the

magnetic structure especially in the ME-relevant incommensurate phases remain unknown. To solve these problems, it is of interest to investigate materials without the additional complexity of the rare earth magnetism. The system $Eu_{1-x}Y_xMnO_3$ is a relevant magnetoelectric compound without rare earth magnetism since Mn^{3+} is the only magnetic ion. In addition, yttrium doping allows a continuous tuning of the magnetoelectric properties in this system and seems to increase the strength of the ME coupling.[28,29]

In this paper, we present detailed investigations of the terahertz spectra of yttrium-doped $Eu_{1-x}Y_xMnO_3$ in the concentration range $0 \leqslant x \leqslant 0.5$. Because the characteristic energies of the magnetoelectric contribution in perovskite manganites lie in the terahertz frequency range, this region is especially important to prove the existence of electromagnons and to study the spectral changes of the ME contribution with doping.

II. EXPERIMENTAL DETAILS

Single crystals of $Eu_{1-x}Y_xMnO_3$ have been grown using the floating-zone method with radiation heating. The samples were characterized using x-ray, magnetic, and dielectric measurements.[28] The transmittance experiments at terahertz frequencies ($3\ cm^{-1} < \nu < 40\ cm^{-1}$) were carried out in a Mach-Zehnder interferometer arrangement,[30] which allows measurements of amplitude and phase shift in a geometry with controlled polarization of the radiation. The absolute values of the complex dielectric permittivity $\varepsilon^* = \varepsilon_1 + i\varepsilon_2$ were determined directly from the measured spectra using the Fresnel optical formulas for the complex transmission coefficient. The experiments in external magnetic fields were performed in a superconducting split-coil magnet with polypropylene windows allowing to carry out transmittance and phase shift experiments in magnetic fields up to 7 T.

Depending upon the specific geometry of the samples, most experiments in external magnetic fields have been carried out in the Faraday geometry ($\mu_0 H \| \vec{k}$, where $\vec{k}$ is the wave vector of light[31]) due to the *ab*-plane orientation of these samples. The field experiments with $x=0.1$ sample (*ac*-plane orientation) have been done in the Voigt geometry ($\mu_0 H \perp \vec{k}$). Although Faraday effect might exist for $\mu_0 H \| \vec{k}$, we do not expect measurable influence on the spectra except close to strong modes of ferromagnetic resonances. These estimates are supported by previous experiments[32] on spin dynamics in Sr-doped $LaMnO_3$. In addition, both Faraday and Voigt geometries have been compared explicitly in $GdMnO_3$, where samples of different orientations were available. Therefore, in the present case, we neglect the influence of Faraday rotation on the terahertz spectra. The investigations of such small effects would require experiment with crossed polarizers and are beyond the scope of the present work.

III. RESULTS

Figure 1 reproduces the phase diagram of Y-doped $EuMnO_3$ from Ref. 28, which has been obtained using structural, magnetic, dielectric, and thermodynamic experiments.

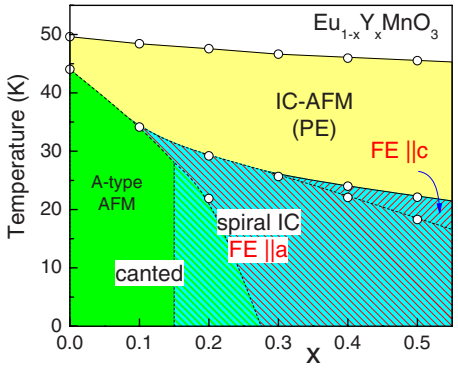

FIG. 1. (Color online) (T-x) phase diagram of $Eu_{1-x}Y_xMnO_3$ reproduced from Ref. 28. The notation of different magnetic phases is given on the basis of magnetization data. AFM, antiferromagnetic phase; IC, incommensurate; PE, paraelectric; FE, ferroelectric. Exact magnetic structures of different phases are still unknown and are indicated in analogy to other perovskite multiferroics.

In the doping range $0 \leqslant x \leqslant 0.5$, $Eu_{1-x}Y_xMnO_3$ orders antiferromagnetically between 45 and 50 K only slightly depending on the yttrium content. From the point of view of the magnetoelectric effect (i.e., changes in dielectric permittivity by magnetic field) and the observation of electromagnons, the phase diagram presented can be divided into four regimes, which we will characterize separately. (i) In the low-doping range $0 \leqslant x \leqslant 0.1$ in the incommensurate (IC) antiferromagnetic (AFM) phase, weak ME effects are observed and the electromagnons are overdamped and not well defined. The IC-AFM phase in this region is followed by the canted (CA) antiferromagnetic phase which shows no magnetoelectric effect. (ii) The phase around $x=0.2$ and at low temperatures is characterized both by the spiral IC-AFM structure (FE$\|a$) and by the existence of a weak ferromagnetism. It therefore reveals the mixture of the CA-AFM properties of lower doping range and of the ferroelectric properties observed for $x \geqslant 0.3$. In this region, the electromagnons are clearly observed in the spectra and can be suppressed by external magnetic fields, which leads to the strong magnetic field dependence of the dielectric permittivity. (iii) For $x \approx 0.3$, the electromagnons are strong in the FE phase at low temperatures but they are not sensitive to external magnetic fields up to 7 T. (iv) The region $0.4 \leqslant x \leqslant 0.5$ is closely similar to $x \approx 0.3$, but here the dielectric permittivity is weakly dependent on the external magnetic field in the narrow temperature range of the competition between ferroelectric phases with electric polarization parallel to a and c axes, respectively.

Within the accuracy of the present experiments, nonzero ME contribution has been observed for $\vec{e} \| a$ axis only and no effects could be detected for other crystallographic directions. Therefore, only the a-axis results will be presented below.

A. Weakly magnetoelectric region ($x \leqslant 0.1$)

The properties of $Eu_{0.9}Y_{0.1}MnO_3$ are representative for this doping range and similar results have been obtained for pure $EuMnO_3$ as well. Figure 2 shows the temperature de-

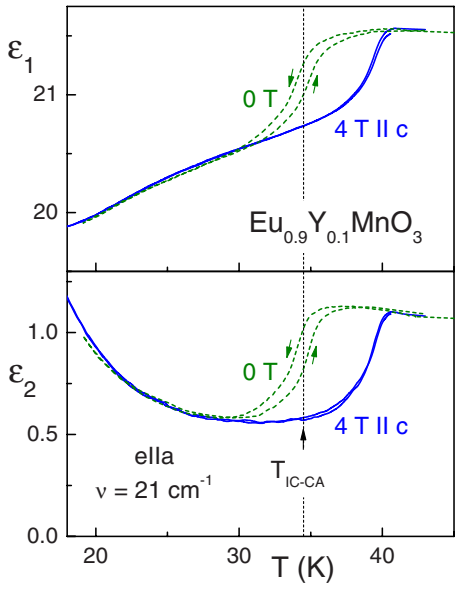

FIG. 2. (Color online) Temperature dependence of the a-axis dielectric permittivity of $Eu_{0.9}Y_{0.1}MnO_3$ in zero external field (green) and at $\mu_0 H=4$ T along the c axis (blue). Upper panel, real part; lower panel, imaginary part. $T_{IC\text{-}CA}$ indicates the transition between the incommensurate and canted antiferromagnetic states. This temperature has been obtained from the magnetization experiments.

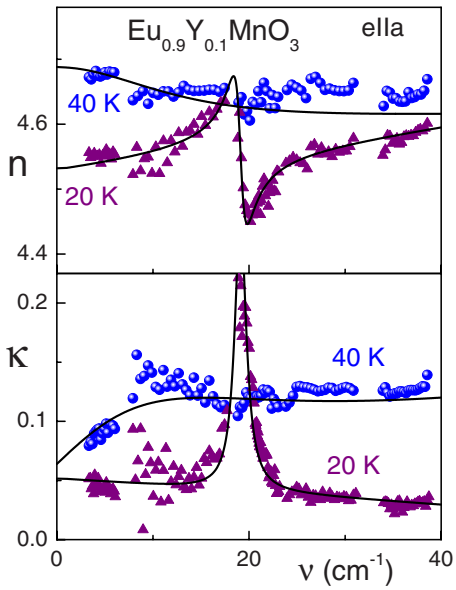

FIG. 3. (Color online) Terahertz spectra of $Eu_{0.9}Y_{0.1}MnO_3$ in incommensurate (40 K data) and canted (20 K data) antiferromagnetic phases. Upper panel, refractive index; lower panel, absorption coefficient. Narrow mode at $\nu \simeq 19$ cm^{-1} represents the antiferromagnetic resonance. Broad additional absorption for $T=40$ K is of magnetoelectric origin. Symbols represent experimental data; lines show the fits using the sum of Lorentzians and a Debye relaxator.

pendence of the dielectric permittivity of $Eu_{0.9}Y_{0.1}MnO_3$ in zero magnetic field and in static field of $\mu_0 H=4$ T parallel to the c axis. The steps in the dielectric constant both in real and imaginary parts are observed close to $T_{IC\text{-}CA} \simeq 34$ K. Higher dielectric constant and stronger absorption in the high-temperature incommensurate magnetic phase reflect the existence of additional contributions from the magnetoelectric interactions. These additional contributions are absent in the CA-AFM phase, which explains the lower dielectric constant below $T_{IC\text{-}CA} \simeq 34$ K. The shift of the IC-CA phase transition by the static field is well seen in this representation. Because the canted antiferromagnetic phase contains a weak ferromagnetic component parallel to the c axis, the application of an external magnetic field in this direction favors the CA-AFM phase and shifts the phase transition to higher temperatures. No such effects have been observed for the other direction of the static magnetic field.

In analogy to the spectral properties of the magnetoelectric phases in $GdMnO_3$ and $TbMnO_3$ where weak but distinct electromagnons exist already in the IC phase,[22] we could expect the existence of characteristic excitations (electromagnons), which govern the magnetoelectric properties in ME materials. In order to prove this similarity, the terahertz spectra of $Eu_{0.9}Y_{0.1}MnO_3$ have been measured in the IC and CA-AFM phases. Typical results of these experiments are shown in Fig. 3. A strong and narrow absorption mode is observed in these spectra close to 19 cm^{-1} in the CA-AFM phase (20 K data). This excitation represents the antiferromagnetic resonance (AFMR), which for the studied polarization of ac magnetic field ($\tilde{h} \| c$, b-cut sample) corresponds to the quasiantiferromagnetic mode of the canted antiferromagnetic phases[33] and is well documented, e.g., in $La_{1-x}Sr_xMnO_3$.[32] The AFMR mode is of magnetic origin and therefore cannot be plotted together with the spectra of dielectric permittivity. Therefore, the (n,κ) representation has been chosen in this case, where $n+i\kappa=\sqrt{\varepsilon^* \mu^*}$. However, far from the AFMR mode at 19 cm^{-1}, the response is purely dielectric ($\mu^* \approx 1$) and the dielectric permittivity is given by $\mathrm{Re}(\varepsilon) \simeq n^2$ and $\mathrm{Im}(\varepsilon) \simeq 2n\kappa$. From these expressions, the absolute values of ε^* at 40 cm^{-1} can be calculated as $\varepsilon^*(40\ \mathrm{K})=21.60+1.20i$ and $\varepsilon^*(20\ \mathrm{K})=21.16+0.29i$. In good approximation, the upper panel of Fig. 3 reflects qualitatively the behavior of ε_1 and the lower panel of ε_2, respectively. Comparing the spectra at 20 K and at 40 K, clear additional contribution can be seen in the magnetoelectric IC phase. This is seen both as a broad absorption in the spectra of $\kappa(\nu)$ and as higher values of the refractive index in the IC phase. Comparing this spectra to those of $GdMnO_3$ and $TbMnO_3$,[22] this additional contribution closely resembles electromagnonlike excitations. However, in the case of $Eu_{0.9}Y_{0.1}MnO_3$, electromagnons are not well defined in energy and are seen as broad contribution only. By fitting the spectra using a Debye-type relaxator (solid lines in Fig. 3, $T=40$ K), the characteristic frequency of the ME excitation in $Eu_{0.9}Y_{0.1}MnO_3$ can be estimated as $\nu \sim 10$ cm^{-1}. Of course, in this case, this characteristic frequency corresponds to an inverse mean lifetime of the excitations.

In the vicinity of the IC-CA transition in $Eu_{0.9}Y_{0.1}MnO_3$, the magnetoelectric contribution is unstable against external magnetic fields along the c axis because the application of the magnetic field in this direction favors the CA-AFM phase. In this temperature range, the ME effects can be ob-

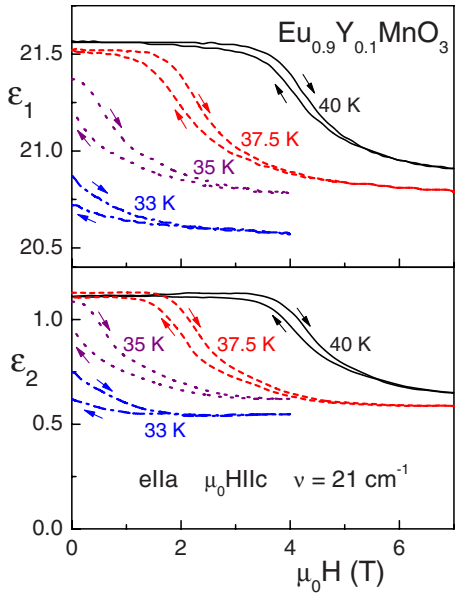

FIG. 4. (Color online) Magnetoelectric effect in $Eu_{0.9}Y_{0.1}MnO_3$ close to the IC-CA transition between two antiferromagnetic phases. Upper panel shows the real part of the dielectric permittivity at ν=21 cm^{-1}, and lower panel the imaginary part.

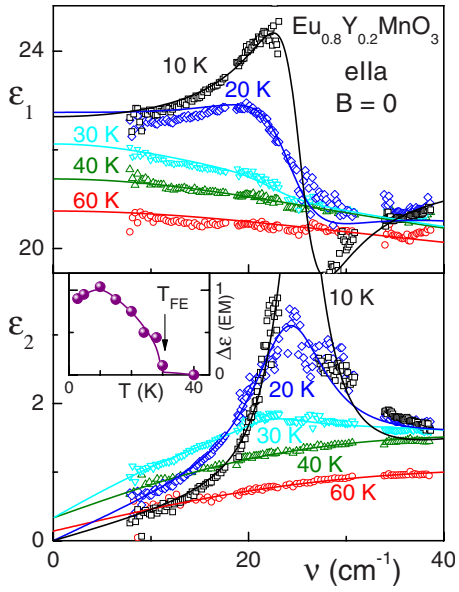

FIG. 5. (Color online) Spectra of the dielectric permittivity along the *a* axis of $Eu_{0.8}Y_{0.2}MnO_3$ in the terahertz frequency range and without external magnetic field. Upper panel, real part; lower panel, imaginary part. Symbols, experiment, lines, Lorentzian fit. Inset shows the dielectric contribution of electromagnon at $\nu \simeq 24$ cm^{-1}.

served at terahertz frequencies. The results of ME experiments are represented in Fig. 4 which shows real and imaginary parts of the dielectric constant as a function of the external magnetic field. In the temperature range 35 K$\lesssim T \lesssim$40 K, the dielectric properties can be easily switched between the values corresponding to IC and CA phases. The observed changes in the permittivity correspond well to the difference between the spectra of both phases, as shown in Fig. 3.

B. Intermediate doping range ($x \sim 0.2$)

For $Eu_{1-x}Y_xMnO_3$ being close to x=0.2, the collinear spin order for $T<T_N$ is not ferroelectric, but for $T\leqslant$29 K, it is followed by a spiral spin structure which induces ferroelectricity with the polarization $P \| a$.[28] It is important to note that this spiral spin structure reveals a ferromagnetic component, probably due to a conical-like distortion.[28] Although the amplitude of the magnetoelectric effects in this compound $\Delta\varepsilon_1(H)$ is only slightly stronger than in $Eu_{0.9}Y_{0.1}MnO_3$, electromagnons can be clearly observed in the spectra and can be well fitted with a Lorentzian with an eigenfrequency close to $\nu \simeq 24$ cm^{-1} (Fig. 5). Figure 5 shows real and imaginary parts of the dielectric spectra of $Eu_{0.8}Y_{0.2}MnO_3$ at different temperatures and in zero external magnetic field. Already with the onset of the collinear IC phase at $T \simeq 48$ K, a broad terahertz absorption starts to grow and marks an approaching of the FE state. The dielectric spectra can be fitted using a Debye relaxator with a characteristic frequency of roughly 25 cm^{-1}. In addition to this broad contribution, a well-defined electromagnon appears in the FE state below T =29 K, which corresponds to the phase transition from the paraelectric (PE) into the FE state. The inset in the lower panel of Fig. 5 shows the dielectric contribution of the electromagnon which exists in the ferroelectric phase only. The growth of the spectral weight of the electromagnon takes place on the costs of the relaxator that nevertheless survives up to the lowest temperatures.

$Eu_{0.8}Y_{0.2}MnO_3$ reveals close similarities with the magnetoelectric properties of $GdMnO_3$ and $TbMnO_3$. This comprises the characteristic frequency of electromagnon and typical values of the dielectric permittivity and includes the possibility to suppress the electromagnon using external magnetic fields. Figure 6 shows the dielectric spectra of $Eu_{0.8}Y_{0.2}MnO_3$ for different external magnetic fields parallel to the *c* axis. Compared to $GdMnO_3$ and $TbMnO_3$, the suppression of the magnetoelectric contribution is more gradual and is not fully finished even at $\mu_0 H$=7 T. This difference could be due to the fact that the FE phase of $Eu_{0.8}Y_{0.2}MnO_3$ exhibits a ferromagnetic component and a different field dependence compared to the pure antiferromagnetic spiral can be expected. In addition, fine structure of the residual absorption is observed in the spectra and can be approximated by two excitations at 21 and 34 cm^{-1}, respectively.

It seems that the spectra of the magnetoelectric perovskite manganites cannot be described using just one single electromagnon and further components can be separated in the spectra. In addition to the splitting of electromagnon observed in Fig. 6, the above-mentioned Debye-type contribution can be seen in all spectra of $Eu_{1-x}Y_xMnO_3$. This contribution was dominating for $Eu_{0.9}Y_{0.1}MnO_3$, and in $Eu_{0.8}Y_{0.2}MnO_3$, it gradually transfers its spectral weight into electromagnons. Complicated spectra of electromagnons have been observed in $TbMnO_3$ as well, both in dielectric permittivity[22] and in inelastic neutron scattering

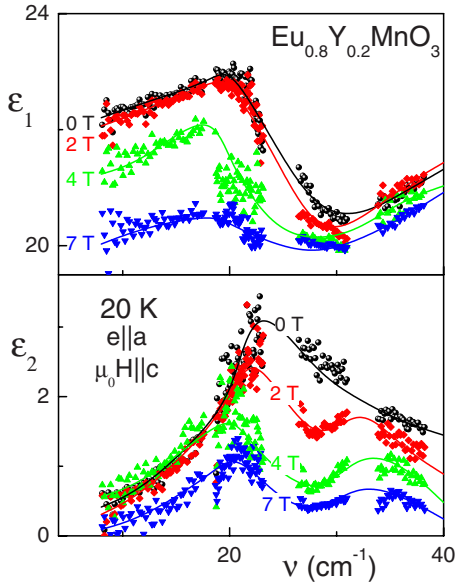

FIG. 6. (Color online) Magnetoelectric effect in $Eu_{0.8}Y_{0.2}MnO_3$: suppression and splitting of electromagnon in external magnetic field in the a-axis dielectric spectra of $Eu_{0.8}Y_{0.2}MnO_3$. Upper panel, real part; lower panel, imaginary part. Symbols, experiment; lines, Lorentzian fit.

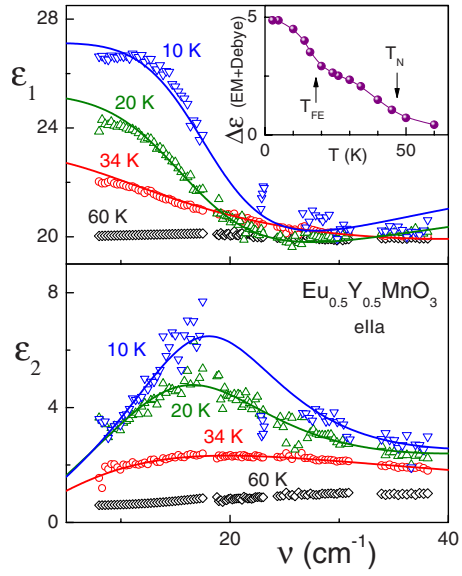

FIG. 7. (Color online) Spectra of dielectric permittivity along the a axis of $Eu_{0.5}Y_{0.5}MnO_3$ in the terahertz frequency range. Upper panel, real part; lower panel, imaginary part. Symbols, experiment; lines, Lorentzian fit. Inset shows the dielectric contribution of the electromagnon and of the Debye relaxator.

experiments.[34] Finally, recent far-infrared experiments in $Eu_{0.75}Y_{0.25}MnO_3$ (Ref. 26) revealed the existence of further electromagnon around $\nu_2=80$ cm^{-1} besides a low-frequency electromagnon at $\nu_1=25$ cm^{-1}.

C. Ferroelectric range ($x \geqslant 0.3$)

In this doping region and in zero external magnetic field, the permittivity spectra similar to $Eu_{0.8}Y_{0.2}MnO_3$ have been observed. A typical example of these spectra is represented in Fig. 7 which shows real and imaginary parts of the dielectric permittivity of $Eu_{0.5}Y_{0.5}MnO_3$ for $\tilde{e}\|a$. Similar to other compositions, broad Debye-type contribution of ME origin can be observed on entering the IC phase. This excitation is getting more pronounced below $T_N \simeq 46$ K and its characteristic damping frequency can be roughly identified as $\Gamma \sim 20$ cm^{-1}. Temperature dependence of this additional magnetoelectric contribution is shown in the inset to the upper frame of Fig. 7. Especially, below the transition from the paraelectric to the ferroelectric phase at $T_{PE/FE} \sim 20$ K, this contribution transforms to a well-defined electromagnon with a characteristic maximum in ε_2 and a step in ε_1 close to 17 cm^{-1} corresponding to its eigenfrequency. The transition to the ferroelectric phase is also seen as a change in slope in the temperature dependence of the dielectric contribution of the electromagnon (inset to Fig. 7). We note that the dielectric contribution of the electromagnons in this composition range is the strongest for the Y-doping range investigated.

For the composition $Eu_{0.7}Y_{0.3}MnO_3$, no magnetic field dependence of the dielectric properties could be observed for external magnetic fields $\mu_0 H \leqslant 7$ T within the experimental accuracy. However, for $x \geqslant 0.4$, a narrow temperature region with $P\|c$ exists (Fig. 1) which can be influenced by magnetic fields $\mu_0 H\|c$. Although this effect is extremely weak, it can be observed in the temperature dependence of the dielectric permittivity. Figure 8 shows the dielectric permittivity of $Eu_{0.5}Y_{0.5}MnO_3$ at $\nu=10$ cm^{-1} as a function of temperature in zero external magnetic field and in a field of 5 T parallel to the c axis. A clear hallmark of the phase transition to the ferroelectric phase with $P\|a$ is seen close to 17 K. This tran-

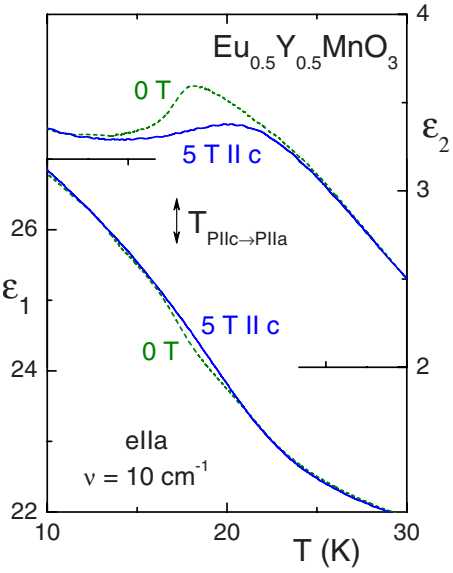

FIG. 8. (Color online) Temperature dependence of the a-axis dielectric permittivity of $Eu_{0.5}Y_{0.5}MnO_3$ in zero external field and at $\mu_0 H=5$ T along the c axis. Upper panel, real part; lower panel, imaginary part. Narrow region close to $T=18$ K, where the permittivity is sensitive to magnetic field, corresponds to the ferroelectric phase with $P\|c$.

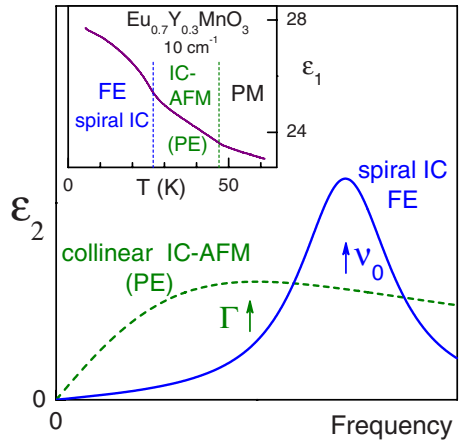

FIG. 9. (Color online) Schematic representation of the terahertz spectra of magnetoelectric manganites. Paramagnetic (PM) phase shows no magnetoelectric contribution; collinear incommensurate-antiferromagnetic (IC-AFM) and paraelectric (PE) phases reveals a broad Debye-type response; in a spiral ferroelectric (IC-FE) phase, well-defined electromagnons are observed. Arrows indicate the damping of the relaxator Γ and the eigenfrequency of the electromagnon ν_0. The inset shows the temperature dependence of the dielectric constant of $Eu_{0.7}Y_{0.3}MnO_3$ at low frequencies as an illustration of the discussed behavior. Changes in slope in the temperature dependence correspond well to the phase transitions to the IC and FE states.

sition is accompanied by a change of the rotation plane of the spiral spin structure from the *bc* plane (with $P\|c$) to the *ab* plane (with $P\|a$). In an external magnetic field with $\mu_0 H\|c$ stabilizing the spiral structure with $P\|a$, the onset of the transition to this phase is shifted to higher temperatures up to $T_{PE/FE}$. This results in a suppression of the $P\|c$ phase and in weak magnetoelectric effects $[\Delta\varepsilon_1(H)/\varepsilon_1(0) \sim 0.8\%$ in the real part of the dielectric permittivity, Fig. 8]. We note, however, that compared to the strong effects for low-doping compositions, the electromagnon contribution is rigid and remains basically stable against the influence of external magnetic fields.

IV. DISCUSSION

Comparing the spectra of the dielectric permittivity of all compositions investigated, several similarities exist in the doping series $Eu_{1-x}Y_xMnO_3$. General behavior of the terahertz spectra is represented schematically in Fig. 9. Broad magnetoelectric contribution exists in the terahertz spectra of the dielectric permittivity in the collinear PE phase in all samples, which seems to result from the same mechanisms as the electromagnon response. This contribution can be described using Debye-type relaxation and is observed already in the paramagnetic phase possibly due to magnonlike fluctuations.

In addition to the broad contribution, a well defined electromagnon starts to grow in the spiral FE state with a doping-dependent resonant frequency which shifts from $\nu \simeq 25\ \mathrm{cm}^{-1}$ for $x=0.2$ to $\nu \simeq 18\ \mathrm{cm}^{-1}$ for $x=0.5$. The dielectric contribution of the electromagnon strongly depends the on the Y concentration and grows from $\Delta\varepsilon \simeq 1$ for $x=0.2$ to $\Delta\varepsilon \simeq 5$ for $x=0.5$. This reflects the increase of the magnetoelectric coupling with the yttrium doping. Indeed, for $x=0.2$, the stabilities of the ferroelectric and the canted states are similar and both phases can be easily switched by external magnetic fields. For $x \geqslant 0.3$, the FE state is stable at low temperature and the electromagnons cannot be influenced by external magnetic fields.

The interplay of different contributions to the dielectric permittivity can be most clearly seen in the temperature dependence of the low-frequency dielectric permittivity. According to the sum rule[35]

$$\varepsilon_1(0) = 1 + \frac{2}{\pi}\int_0^\infty \frac{\varepsilon_2(\omega)}{\omega} d\omega, \tag{1}$$

the low-frequency dielectric permittivity is a measure of all high-frequency contributions. The inset in Fig. 9 shows the temperature dependence of ε_1 in $Eu_{0.7}Y_{0.3}MnO_3$ at $\nu = 10\ \mathrm{cm}^{-1}$, i.e., below all excitations observed in the terahertz spectra. On cooling the sample through $T_N=48$ K, the increase in the slope of $\varepsilon_1(T)$ reflects the growth of the Debye-type excitation in the collinear PE state. On further cooling, the spiral FE state is reached where well-defined electromagnons are observed. The appearance of this contribution is seen as a change in slope of $\varepsilon_1(T)$ at T_{FE}.

Finally, the spectra of electromagnons reveal a distinct fine structure. This is most clearly documented in Fig. 6 and correlates well with other experimental observations both in $TbMnO_3$ (Ref. 34) and in $Eu_{0.75}Y_{0.25}MnO_3$.[26]

V. CONCLUSIONS

Dielectric properties of yttrium-doped $EuMnO_3$ in the composition range $0 \leqslant x \leqslant 0.5$ have been investigated in the terahertz frequency range. Nonzero magnetoelectric contribution to the dielectric permittivity can be observed in all compositions for $\tilde{e}\|a$ only. In the low-doping range with coexisting incommensurate and canted antiferromagnetic states ($x \leqslant 0.2$), the dielectric properties can be modified by external magnetic field parallel to the *c* axis especially on the border line between these two phases. Large magnetoelectric effects can be observed in this doping range and at terahertz frequencies. Well-defined electromagnons are observed for $x \geqslant 0.2$ close to $\nu \sim 20\ \mathrm{cm}^{-1}$ and with strongly doping-dependent dielectric strength. In addition to electromagnons, a broad Debye-type contribution of magnetoelectric origin is observed for all compositions. Most naturally, this contribution can be explained as a heavily overdamped electromagnon that already exists in the collinear spin state.

ACKNOWLEDGMENTS

This work has been partly supported by DFG (SFB 484) and by RFBR (04-02-16592 and 06-02-17514).

[1] P. Curie, J. Phys. Theor. Appl. **3**, 393 (1894).
[2] L. D. Landau and E. M. Lifshitz, *Electrodynamics of Contineous Media* (Pergamon, Oxford, 1960).
[3] I. E. Dzyaloshinskii, Sov. Phys. JETP **10**, 628, 1959.
[4] D. N. Astrov, Sov. Phys. JETP **11**, 708 (1960).
[5] G. A. Smolenskiĭ and I. E. Chupis, Sov. Phys. Usp. **25**, 475 (1982).
[6] O'Dell, *The Electrodynamics of Magneto-Electric Media* (North-Holland, Amsterdam, 1970).
[7] M. Fiebig, J. Phys. D **38**, R123 (2005).
[8] D. Khomskii, J. Magn. Magn. Mater. **306**, 1 (2006).
[9] S.-W. Cheong and M. Mostovoy, Nat. Mater. **6**, 13 (2007).
[10] W. Eerenstein, N. D. Mathur, and J. F. Scott, Nature (London) **442**, 759 (2006).
[11] G. Lawes, A. B. Harris, T. Kimura, N. Rogado, R. J. Cava, A. Aharony, O. Entin-Wohlman, T. Yildrim, M. Kenzelmann, C. Broholm, and A. P. Ramirez, Phys. Rev. Lett. **95**, 087205 (2005).
[12] T. Kimura, T. Goto, H. Shintani, K. Ishizaka, T. Arima, and Y. Tokura, Nature (London) **426**, 55 (2003).
[13] T. Kimura, G. Lawes, T. Goto, Y. Tokura, and A. P. Ramirez, Phys. Rev. B **71**, 224425 (2005).
[14] M. Kenzelmann, A. B. Harris, S. Jonas, C. Broholm, J. Schefer, S. B. Kim, C. L. Zhang, S.-W. Cheong, O. P. Vajk, and J. W. Lynn, Phys. Rev. Lett. **95**, 087206 (2005).
[15] T. Arima, A. Tokunaga, T. Goto, H. Kimura, Y. Noda, and Y. Tokura, Phys. Rev. Lett. **96**, 097202 (2006).
[16] H. Katsura, N. Nagaosa, and A. V. Balatsky, Phys. Rev. Lett. **95**, 057205 (2005).
[17] M. Mostovoy, Phys. Rev. Lett. **96**, 067601 (2006).
[18] I. A. Sergienko and E. Dagotto, Phys. Rev. B **73**, 094434 (2006).
[19] H. Schmid, Ferroelectrics **62**, 317 (1994).
[20] V. G. Bar'yakhtar and I. E. Chupis, Sov. Phys. Solid State **11**, 2628 (1970).
[21] H. Katsura, A. V. Balatsky, and N. Nagaosa, Phys. Rev. Lett. **98**, 027203 (2007).
[22] A. Pimenov, A. A. Mukhin, V. Yu. Ivanov, V. D. Travkin, A. M. Balbashov, and A. Loidl, Nat. Phys. **2**, 97 (2006).
[23] A. B. Sushkov, R. V. Aguilar, S. Park, S.-W. Cheong, and H. D. Drew, Phys. Rev. Lett. **98**, 027202 (2007).
[24] A. Pimenov, T. Rudolf, F. Mayr, A. Loidl, A. A. Mukhin, and A. M. Balbashov, Phys. Rev. B **74**, 100403(R) (2006).
[25] I. E. Chupis, Low Temp. Phys. **33**, 715 (2007).
[26] R. V. Aguilar, A. B. Sushkov, C. L. Zhang, Y.-J. Choi, S.-W. Cheong, and H. D. Drew, Phys. Rev. B **76**, 060404(R) (2007).
[27] J. Hemberger, S. Lobina, H.-A. Krug von Nidda, N. Tristan, V. Yu. Ivanov, A. A. Mukhin, A. M. Balbashov, and A. Loidl, Phys. Rev. B **70**, 024414 (2004).
[28] J. Hemberger, F. Schrettle, A. Pimenov, P. Lunkenheimer, V. Yu. Ivanov, A. A. Mukhin, A. M. Balbashov, and A. Loidl, Phys. Rev. B **75**, 035118 (2007).
[29] V. Yu. Ivanov, A. A. Mukhin, V. D. Travkin, A. S. Prokhorov, A. M. Kadomtsev, Yu. F. Popov, G. P. Vorobev, K. I. Kamilov, and A. M. Balbashov, J. Magn. Magn. Mater. **300**, e130 (2006).
[30] A. A. Volkov, Yu. G. Goncharov, G. V. Kozlov, S. P. Lebedev, and A. M. Prochorov, Infrared Phys. **25**, 369 (1985); A. Pimenov, S. Tachos, T. Rudolf, A. Loidl, D. Schrupp, M. Sing, R. Claessen, and V. A. M. Brabers, Phys. Rev. B **72**, 035131 (2005).
[31] A. K. Zvezdin and V. A. Kotov, *Modern Magnetooptics and Magnetooptical Materials* (Institute of Physics, Bristol, 1997).
[32] D. Ivannikov, M. Biberacher, H.-A. Krug von Nidda, A. Pimenov, A. Loidl, A. A. Mukhin, and A. M. Balbashov, Phys. Rev. B **65**, 214422 (2002).
[33] A. A. Mukhin, A. Pimenov, M. Biberacher, and A. Loidl, J. Magn. Reson. **170**, 8 (2004).
[34] D. Senff, P. Link, K. Hradil, A. Hiess, L. P. Regnault, Y. Sidis, N. Aliouane, D. N. Argyriou, and M. Braden, Phys. Rev. Lett. **98**, 137206 (2007).
[35] M. Dressel and G. Grüner, *Electrodynamics of Solids: Optical Properties of Electrons in Matter* (Cambridge University Press, Cambridge, 2002), p. 67.